Optimization of Airfoils for Maximum Lift

ROBERT H. LIEBECK*
Douglas Aircraft Company, Long Beach, Calif.
AND
ALLEN I. ORMSBEE†
University of Illinois, Urbana, Ill.

The pressure distribution which provides the maximum lift without separation for a monoelement airfoil in an incompressible flow is determined using existing boundary-layer theory and the calculus of variations. The airfoil profiles corresponding to these pressure distributions are determined using second-order airfoil theory. The results indicate maximum lift coefficients as high as 2.8 for Reynolds numbers between five and ten million, and the corresponding drag coefficients are on the order of 0.01. Compressibility has not been considered directly, however the form of the optimum pressure distributions suggests that the critical Mach numbers should be on the order of 0.35.

Nomenclature

c	=	airfoil chord
C_L	=	airfoil section lift coefficient, $C_L = L/\frac{1}{2}\rho V_\infty{}^2 c$
C_{Lu}	=	upper-surface lift coefficient
C_D	=	airfoil section drag coefficient, $C_D = D/\frac{1}{2}\rho V_\infty{}^2 c$
C_{Dl}	=	lower-surface drag coefficient
C_{Du}	=	upper-surface drag coefficient
C_p	=	pressure coefficient, $C_p = (p - p_\infty)/\frac{1}{2}\rho V_\infty{}^2$
$C_{p\ \min}$	=	minimum value of C_p on upper surface of the airfoil
C_{pl}	=	defined in Fig. 7
$\bar{C}_p$	=	modified pressure coefficient $\bar{C}_p = (p - p_0)/\frac{1}{2}\rho V_0{}^2$
I_s	=	function defined by Eqs. (12) and (15)
k_l	=	defined by Eq. (9)
k_{lp}	=	defined by Eq. (14)
k_{lr}	=	defined by Eq. (14)
k_l	=	defined by Eq. (9)
p	=	static pressure
Re_∞	=	freestream Reynolds number, $Re_\infty = V_\infty c/\nu$
Re_{x_0}	=	Reynolds number defined by $Re_{x_0} = V_0 x_0/\nu$
V	=	velocity on the airfoil surface
X,x	=	Cartesian coordinate (see Figs. 3 and 4)
X_1,X_2,X_3	=	defined in Fig. 7
z	=	defined by $z = x/x_0$
Z	=	value of z at airfoil trailing edge
α	=	airfoil angle of attack
ν	=	kinematic viscosity
ρ	=	density

Subscripts

te	=	condition at airfoil trailing edge
u	=	airfoil upper surface
y	=	differentiation with respect to y
o	=	conditions when $C_p = C_{p\ \min}$ on airfoil upper surface
∞	=	freestream conditions

Presented as Paper 69-739 at the CASI/AIAA Subsonic Aero- and Hydro-Dynamics Meeting, Ottawa, Canada, July 2–3, 1969; submitted July 31, 1969; revision received January 20, 1970. Appreciation is expressed to A. M. O. Smith for suggesting the problem, and to P. B. S. Lissaman of the California Institute of Technology (a Consultant for Douglas) for many helpful ideas and suggestions. In addition, appreciation is expressed to the Boeing Company for financial assistance in support of this research provided by the Boeing Grant for Doctoral Dissertations in Aeronautics.

* Senior Engineer/Scientist, Aerodynamics Research Group; formerly Instructor at the University of Illinois. Member AIAA.
† Professor, Aeronautical and Astronautical Engineering Department. Associate Fellow AIAA.

1. Introduction

AN optimization procedure is developed to determine the maximum lift which may be carried by a monoelement airfoil. Well established boundary-layer and airfoil analysis methods are used, and the flow is assumed steady, two dimensional, and incompressible.

The problem can be divided into two related subproblems: the viscous problem of obtaining a pressure distribution which provides the maximum lift without separation, and the inviscid problem of determining the particular airfoil which corresponds to the desired pressure distribution. These two problems are coupled since a particular pressure distribution may not provide a physically possible or structurally practical airfoil.

The lift coefficient in terms of the pressure coefficient is given by

$$C_L = \left[\int_0^c C_p \frac{dx}{c}\right]_{\substack{\text{lower}\\\text{surface}}} - \left[\int_0^c C_p \frac{dx}{c}\right]_{\substack{\text{upper}\\\text{surface}}}$$

where the freestream is aligned with the x axis. The lower-surface contribution has a maximum when $C_p = 1$, although evidently complete stagnation can only occur at a single point near the leading edge. The upper-surface contribution is limited by boundary-layer separation because of the adverse pressure gradients. In addition, the pressure distribution must be continuous at the leading and trailing edges. The procedure will be to optimize the pressure distribution for maximum lift while satisfying these constraints, and then modify the result in order to obtain an acceptable shape.

2. Formulation and Solution

2.1 General Form of the Upper-Surface Pressure Distribution

Referring to Fig. 1, the upper-surface pressure distribution will initially be taken to be made up of two basic regions: 1) a region of acceleration from the leading-edge stagnation point to the maximum velocity ($C_{p\ \min}$) and 2) a pressure recovery region from $C_{p\ \min}$ to the trailing-edge pressure coefficient C_{pte}. Two cases will be considered a) a turbulent boundary layer over the entire upper surface and b) a laminar boundary layer in region 1 with instantaneous transition at the point of maximum velocity to a turbulent boundary layer in region 2. Thus, cases a and b are distinguished

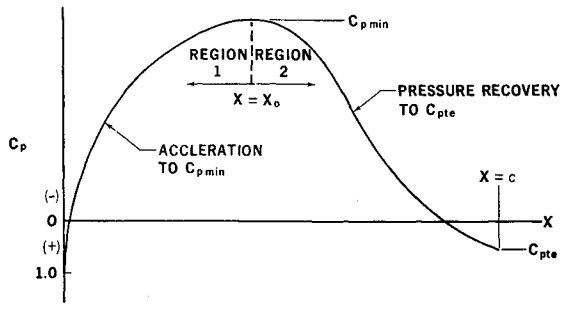

Fig. 1 General form for upper-surface pressure distribution.

by the different state of the boundary layer at the start of the pressure rise region.

2.2 Separation

In order to shape the pressure recovery region, it is necessary to have a method for testing for boundary-layer separation. Stratford's paper[1] does this and provides a basis for the precise determination of the entire pressure recovery region, giving a distribution which just avoids separation along its entire length. The basic result is derived for a pressure distribution of the form shown in Fig 2, where the boundary layer is taken to be turbulent over the entire region. Defining

$$\bar{C}_p = (p - p_0)/\tfrac{1}{2}\rho V_0^2 \quad \text{and} \quad Re_{x0} = V_0 x_0/\nu \tag{1}$$

the basic result of Ref. 1 is given by

$$\bar{C}_p(x/x_0) = 0.49\{(Re_{x0})^{1/5}[(x/x_0)^{1/5} - 1]\}^{1/3},\ \bar{C}_p \leq \tfrac{4}{7} \tag{2}$$

For pressure recovery beyond $\bar{C}_p = \frac{4}{7}$, Stratford suggests using a constant form parameter solution with zero shearing stress at the wall. This yields, for a form parameter of 2 as suggested by Stratford,

$$\bar{C}_p(x/x_0) = 1 - \{a/[(x/x_0) + b]^{1/2}\},\ \bar{C}_p > \tfrac{4}{7} \tag{3}$$

where the constants a and b are chosen to match $\bar{C}_p$ and its derivative when $\bar{C}_p = \frac{4}{7}$. Equations (2) and (3) define the imminent separation pressure recovery distribution of Fig. 2.

The airfoil problem requires a stagnation near $X = 0$ with the velocity monotonically increasing to V_0 at $X = X_0$ as suggested in Fig. 1. Stratford has provided two straightforward relations which modify the previous result to account for an initial region of favorable pressure gradient where the boundary layer may be laminar or turbulent by using an effective origin x_0 in Eqs. (2) and (3). For a favorable gradient with a turbulent boundary layer, this gives

$$x_0 = \int_0^{X_0} \left(\frac{V}{V_0}\right)^3 dX \tag{4}$$

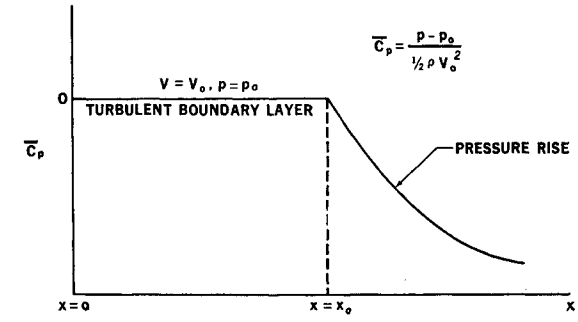

Fig. 2 Pressure distribuiton used by Stratford (Ref. 2).

while for a laminar boundary layer, it yields

$$x_0 = 38.2(Re_{x0})^{-3/8}\left[\int_0^{X_0}\left(\frac{V}{V_0}\right)^5 d\left(\frac{X}{X_0}\right)\right]^{5/8} X_0 \tag{5}$$

X is the distance from the actual leading edge, and x is the distance from the effective leading edge on which Eqs. (2) and (3) are based.

2.3 Application of Stratford's Result to the Airfoil Problem

Stratford's result provides a pressure distribution which recovers a given pressure difference in the shortest possible distance. As applied to the maximum lift problem, this means that for a given pressure difference $C_{pte} - C_{p\,min}$, the chordwise position of $C_{p\,min}$ can be located as far aft as possible by using the Stratford pressure recovery distribution. Certain modifications are necessary, however, before it becomes usable in the present problem.

Defining the conventional pressure coefficient as

$$C_p = (p - p_\infty)/\tfrac{1}{2}\rho V_\infty^2$$

and using Eq. (1), the relation

$$C_p = (V_0/V_\infty)^2(\bar{C}_p - 1) + 1$$

is obtained. Conditions at the trailing edge give

$$(V_0/V_\infty)^2 = C_{pte} - 1/\bar{C}_{pte} - 1 \tag{6}$$

so that the relation between C_p and $\bar{C}_p$ may be written as

$$C_p = [(1 - C_{pte})/(1 - \bar{C}_{pte})](\bar{C}_p - 1) + 1 \tag{7}$$

Similarly, Re_{x0} is related to the freestream Reynolds number Re_∞ by

$$Re_{x0} = \frac{V_0}{V_\infty}\frac{x_0}{c}Re_\infty = \left(\frac{C_{pte} - 1}{\bar{C}_{pte} - 1}\right)^{1/2}\frac{x_0}{c}Re_\infty \tag{8}$$

For a given pressure distribution from $X = 0$ to $X = X_0$, Eqs. (4) and (5) may be considered as having the forms

$$\begin{aligned} X_0 &= k_t x_0, \qquad k_t \geq 1 \\ X_0 &= k_l x_0, \qquad k_l > 1 \end{aligned} \tag{9}$$

for case a and case b, respectively, where k_t and k_l are constants. For the analysis which follows, it will be convenient to define a new independent variable for Eqs. (2) and (3) as $z = x/x_0$ whose value at the trailing edge is $Z = (x/x_0)_{te}$.

2.4 Proposed Upper-Surface Pressure Distributions

A more specific form for the upper-surface pressure distribution may now be examined using the Stratford distribution for the pressure recovery region. Figure 3 describes the proposed pressure distribution for case a. An arbitrary favorable pressure gradient rooftop is assumed for the region from $X = 0$ to $X = X_0$, and the Stratford distribution is assumed from $X = X_0$ to $X = c$. Using the relation $X_0 =$

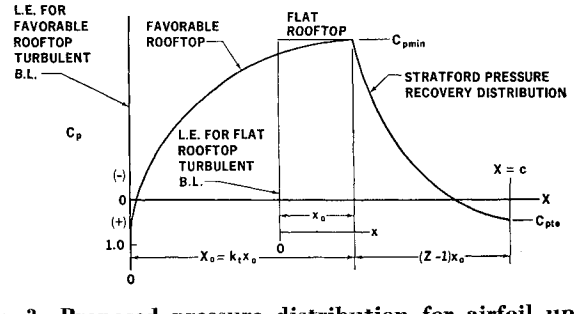

Fig. 3 Proposed pressure distribution for airfoil upper surface with entire boundary-layer turbulent (not to scale).

$k_t x_0$, Eq. (4) is rewritten in terms of the pressure coefficient as

$$1 = \int_0^{k_t} \left(\frac{1 - C_p}{1 - C_{p\,\min}}\right)^{3/2} d\left(\frac{X}{x_0}\right) \tag{10}$$

Since $C_p \geq C_{p\,\min}$, as the pressure distribution from $X = 0$ to $X = X_0$ approaches a flat rooftop ($C_p = \text{const} = C_{p\,\min}$), then $X_0 \to x_0$ and $k_t \to 1$.

The distance from $X = X_0$ to $X = c$ is determined by the values of Z and C_{pte}. This can be demonstrated by using Eq. (6) and writing

$$C_{p\,\min} = 1 - (V_0^2/V_\infty^2) = 1 - (C_{pte} - 1)/(\bar{C}_{pte} - 1) \tag{11}$$

and recalling that $\bar{C}_{pte}$ is determined from Eqs. (2) and (3) when $z = (x/x_0)_{te} = Z$. Zx_0 represents the distance from $X = X_0$ to $X = c$ for the arbitrary rooftop distribution, as can be seen from Fig. 3.

The lift coefficient for the upper surface is given by

$$C_{Lu} = -\left[\int_0^{k_t} C_p\, d\left(\frac{X}{x_0}\right) + \int_{k_t}^{(k_t+Z-1)} C_p\, d\left(\frac{X}{x_0}\right)\right] \Big/ (k_t + Z - 1)$$

where, from Fig. 3, the chord is $c = (k_t + Z - 1)x_0$. The second integral in the previous equation represents the contribution to C_{Lu} from the Stratford recovery portion of the pressure distribution. In this region, C_p is given by Eqs. (2), (3), and (7) as a function of $z = x/x_0$ and the three parameters Re_{x0}, C_{pte}, and Z. Furthermore, from Fig. 3, $z = X/x_0 - (k_t - 1)$ and $dz = d(X/x_0)$, therefore,

$$\int_{k_t}^{(k_t+Z-1)} C_p\, d\left(\frac{X}{x_0}\right) = \int_1^Z \times C_p(z,C_{pte},Re_{x0})dz = I_s(Z,C_{pte},Re_{x0}) \tag{12}$$

The expression for C_{Lu} now becomes

$$C_{Lu} = -\left[\int_0^{k_t} C_p\, d\left(\frac{X}{x_0}\right) + I_s(Z,C_{pte},Re_{x0})\right] \Big/ (k_t + Z - 1) \tag{13}$$

Equations (10) and (13) define C_{Lu} for case a as a function of the pressure distribution from $X = 0$ to $X = X_0$, and the parameters Z, C_{pte}, and Re_{x0}, where $C_{p\,\min}$ is given by Eq. (11). It remains to determine the optimum distribution and values of the parameters.

The development of the equivalent of Eqs. (10) and (13) for case b is quite similar to that of case a. The proposed pressure distribution for case b is shown in Fig. 4. An arbitrary favorable rooftop is assumed for the region from $X = 0$ to $X = X_0$, however, in this case the boundary layer in this region is assumed to be laminar. Instantaneous transition at $X = X_0$ is assumed, and again the Stratford recovery is prescribed from $X = X_0$ to $X = c$. The same relationships for C_{pte}, Re_{x0}, z, and $C_{p\,\min}$ apply here to case b as were discussed earlier for case a, and again Z, C_{pte}, and Re_{x0} are not specified at this time.

It is convenient to rewrite Eq. (5) in the form $X_0 = k_{lp}(k_{lr}x_0)$ where

$$k_{lr} = (Re_{x0})^{3/8}/38.2 > 1$$
$$k_{lp} = \left[\int_0^{X_0} \left(\frac{1 - C_p}{1 - C_{p\,\min}}\right)^{5/2} d\left(\frac{X}{X_0}\right)\right]^{-5/8} \geq 1 \tag{14}$$

k_{lr} is a function of Re_{x0} only. The existence of a laminar instead of a turbulent boundary layer from $X = 0$ to $X = X_0$ implies an increase in the distance X_0, and k_{lr} accounts for this as shown in Fig. 4. k_{lp} is dependent on the pressure distribution from $X = 0$ to $X = X_0$, and has an effect on the distance X_0 which is quite similar to k_t of case a.

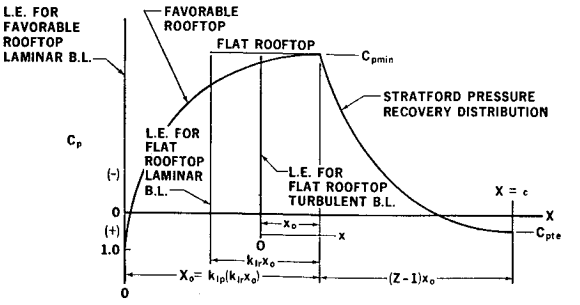

Fig. 4 Proposed pressure distribution for airfoil upper surface with boundary-layer laminar from $X = 0$ to $X = X_0$, and turbulent from $X = X_0$ to $X = c$ (not to scale).

Referring to Fig. 4, the chordlength for case b is $c = (k_{lp}k_{lr} + Z - 1)x_0$, and the upper-surface lift coefficient is given by

$$C_{Lu} = -\left[\int_0^{k_{lp}k_{lr}} C_p\, d\left(\frac{X}{x_0}\right) + \int_{k_{lp}k_{lr}}^{k_{lp}k_{lr}+Z-1} C_p\, d\left(\frac{X}{x_0}\right)\right] \Big/ (k_{lp}k_{lr} + Z - 1)$$

Also, from Fig. 4,

$$z = (X/x_0) - (k_{lp}k_{lr} - 1), \qquad dz = d(X/x_0)$$

and therefore

$$\int_{k_{lp}k_{lr}}^{k_{lp}k_{lr}+Z-1} C_p\, d\left(\frac{X}{x_0}\right) = \int_1^Z \times C_p(z;C_{pte},Re_{x0})dz = I_s(Z,C_{pte},Re_{x0}) \tag{15}$$

The functions I_s of Eqs. (12) and (15) are seen to be identical, and the expression for C_{Lu} for case b is now given by

$$C_{Lu} = -\left[\int_0^{k_{lp}k_{lr}} C_p\, d\left(\frac{X}{x_0}\right) + I_s(Z,C_{pte},Re_{x0})\right] \Big/ (k_{lp}k_{lr} + Z - 1) \tag{16}$$

k_{lp} is more conveniently defined by rewriting Eq. (14) as

$$\frac{k_{lr}}{k_{lp}^{3/5}} = \int_0^{k_{lp}k_{lr}} \left(\frac{1 - C_p}{1 - C_{p\,\min}}\right)^{5/2} d\left(\frac{X}{x_0}\right) \tag{17}$$

Equations (16) and (17) define C_{Lu} for case b as a function of the pressure distribution from $X = 0$ to $X = X_0$ and the parameters Z, C_{pte}, and Re_{x0}.

2.5 Application of the Calculus of Variations to Maximize C_{Lu}

The form of the equations which specify C_{Lu} for both cases a and b suggests the use of the calculus of variations to determine the function $C_p(X)$ and the parameters Z, C_{pte}, and Re_{x0} which maximize C_{Lu}. For given values of C_{pte} and Re_{x0}, Eqs. (10) and (13) of case a, and Eqs. (16) and (17) of case b define a problem of the form

$$\text{Maximize } H[y(x);K,N] = \left[\int_0^K f[y(x)]dx + J(N)\right] \Big/ G_2(K,N) \tag{18}$$

with the constraint

$$G(K,N) + \int_0^K g[y(x)]dx = 0 \tag{19}$$

That is, it is desired to find the function $y(x)$ and the values of K and N which maximize the functional H subject to the

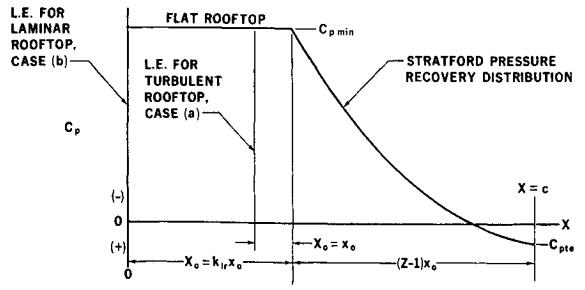

Fig. 5 Optimum pressure distribution for airfoil upper surface, case a and case b (not to scale).

constraint given by Eq. (19), where the functions $f(y)$, $J(N)$, $G_2(K,N)$, $G(N)$, and $g(y)$ are known. Introducing the Lagrange multiplier λ, Eqs. (18) and (19) may be combined in the form

$$\bar{H}[y(x);K,N,\lambda] = \left\{\int_0^K [f + \lambda g]dx + J(N) + \lambda G(K,N)\right\} \Big/ G_2(K,N)$$

and letting $G_1(K,N,\lambda) = J(N) + \lambda G(K,N)$ and

$$I[y(x);K,\lambda] = \int_0^K (f + \lambda g)dx$$

this becomes

$$\bar{H}[y(x);K,N,\lambda] = \{I[y(x);K,\lambda] + G_1(K,N,\lambda)\}/G_2(K,N)$$

The first variation of $\bar{H}$ is

$$\delta\bar{H} = (\partial\bar{H}/\partial I)\delta I + (\partial\bar{H}/\partial G_1)\delta G_1 + (\partial\bar{H}/\partial G_2)\delta G_2 \quad (20)$$

$\delta\bar{H} = 0$ is a necessary condition for an extremum of $\bar{H}$. The second variation of $\bar{H}$ is

$$\delta^2\bar{H} = \frac{\partial^2\bar{H}}{\partial I^2}(\delta I)^2 + \frac{\partial^2\bar{H}}{\partial G_1^2}(\delta G_1)^2 + \frac{\partial^2\bar{H}}{\partial G_2}(\delta G_2)^2 + \left(\frac{\partial^2\bar{H}}{\partial I\partial G_1} + \frac{\partial^2\bar{H}}{\partial G_1\partial I}\right)\delta I\delta G_1 + \left(\frac{\partial^2\bar{H}}{\partial I\partial G_2} + \frac{\partial^2\bar{H}}{\partial G_2\partial I}\right)\delta I\delta G_2 + \left(\frac{\partial^2\bar{H}}{\partial G_1\partial G_2} + \frac{\partial^2\bar{H}}{\partial G_2\partial G_1}\right)\delta G_1\delta G_2 + \frac{\partial\bar{H}}{\partial I}\delta^2 I + \frac{\partial\bar{H}}{\partial G_1}\delta^2 G_1 + \frac{\partial\bar{H}}{\partial G_2}\delta^2 G_2 \quad (21)$$

and the condition for a maximum is $\delta^2\bar{H} \leq 0$. It is important to note that on an extremum, the partial derivatives ($\partial\bar{H}/\partial I$, $\partial\bar{H}/\partial G_1$, $\partial^2\bar{H}/\partial I^2$, $\partial^2\bar{H}/\partial I\partial G_1$, . . .) of Eqs. (20) and (21) are constants, and the actual variation is accounted for by the variations [δI, δG_1, $(\delta I)^2$, $\delta^2 I$, . . .].

The variation δI is given by

$$\delta I = \int_0^K (f_y + \lambda g_y)\delta y dx + (f + \lambda g)\Big|_{x=K}\delta K \quad (22)$$

for arbitrary variations δy and δK, and the variations δG_1 and δG_2 are given by

$$\delta G_1 = (\partial G_1/\partial K)\delta K + (\partial G_1/\partial N)\delta N \quad (23)$$

$$\delta G_2 = (\partial G_2/\partial K)\delta K + (\partial G_2/\partial N)\delta N \quad (24)$$

for arbitrary variations δK and δN.

Using Eqs. (22), (23), and (24), Eq. (20) becomes

$$\delta\bar{H} = \frac{\partial\bar{H}}{\partial I}\int_0^K (f_y + \lambda g_y)\delta y dx + \left[\frac{\partial\bar{H}}{\partial I}(f + \lambda g)\Big|_{x=K} + \frac{\partial\bar{H}}{\partial G_1}\frac{\partial G_1}{\partial K} + \frac{\partial\bar{H}}{\partial G_2}\frac{\partial G_2}{\partial K}\right]\delta K + \left[\frac{\partial\bar{H}}{\partial G_1}\frac{\partial G_1}{\partial N} + \frac{\partial\bar{H}}{\partial G_2}\frac{\partial G_2}{\partial N}\right]\delta N = 0 \quad (25)$$

Since $\delta\bar{H}$ must vanish for every admissible set of variations δy, δK, and δN, Eq. (25) breaks up into the three separate conditions

$$f_y + \lambda g_y = 0 \quad (26)$$

$$\frac{\partial\bar{H}}{\partial I}(f + \lambda g)\Big|_{x=K} + \frac{\partial\bar{H}}{\partial G_1}\frac{\partial G_1}{\partial K} + \frac{\partial\bar{H}}{\partial G_2}\frac{\partial G_2}{\partial K} = 0 \quad (27)$$

$$(\partial\bar{H}/\partial G_1)\,\partial G_1/\partial N + (\partial\bar{H}/\partial G_2)\,\partial G_2/\partial N = 0 \quad (28)$$

where Eq. (26) is the Euler equation for δy, Eq. (27) is the transversality condition for δK, and Eq. (28) represents the vanishing of the derivative of $\bar{H}$ with respect to N.

Applying Eq. (26) to Eqs. (10) and (13) of case 2 yields

$$-1 + \tfrac{3}{2}\lambda(1 - C_p)^{1/2} = 0 \quad (29)$$

which indicates that the solution $C_p(X)$ from $X = 0$ to $X = X_0$ is a constant. Therefore,

$$C_p(X) = C_{p\,min}, \qquad (0 \leq X \leq X_0)$$

since continuity requires $C_p(X_0) = C_{p\,min}$, and thus, from Eq. (10), $k_t = 1$. This means that the only admissible variation of k_t is $\delta k_t = 0$, and therefore it is not necessary to satisfy Eq. (27). In order for the previous solution to provide a maximum of C_{Lu}, it must satisfy $\delta^2\bar{H} \leq 0$ where $\delta^2\bar{H}$ is given by Eq. (21). Since $\delta I = 0$ and $\delta k_t = 0$, Eq. (21) reduces to the two conditions

$$\delta^2 I \leq 0 \Rightarrow f_{yy} + \lambda g_{yy} \leq 0 \quad (30)$$

$$\partial^2\bar{H}/\partial N^2 \leq 0 \quad (31)$$

Referring to Eq. (30),

$$f_{yy} + \lambda g_{yy} = -\tfrac{3}{4}\lambda(1 - C_p)^{-1/2} = -\tfrac{3}{4}\lambda(1 - C_{p\,min})^{-1/2}$$

This quantity is negative since $C_{p\,min}$ is negative, and from Eqs. (10) and (29), λ is positive. Before applying Eqs. (28) and (31) to determine the optimum value of N (Z in the actual problem), it will be convenient to apply the previous procedure to case b.

Application of Eq. (26) to Eqs. (16) and (17) of case b yields

$$-1 + \tfrac{5}{2}(1 - C_p)^{3/2} = 0 \quad (32)$$

which gives

$$C_p(X) = C_{p\,min}, \qquad (0 \leq X \leq X_0)$$

as in case a, and therefore the only admissible variation of k_{lp} is $\delta k_{lp} = 0$, and thus, Eq. (27) need not be satisfied. Referring to Eq. (30) once again

$$f_{yy} = \lambda g_{yy} = -\tfrac{15}{4}\lambda(1 - C_{p\,min})^{1/2}$$

which is always negative as in case a.

Referring to Fig. 5, C_{Lu} may now be written in the form

$$C_{Lu} = -[C_{p\,min}k_{lr} + I_s(Z,C_{pte},Re_{x0})]/(Z + k_{lr} - 1)$$

where $k_{lr} = 1$ for case a, and k_{lr} is given by Eq. (14) for case b. $C_{p\,min}$ as a function of Z is obtained from Eq. (11) as

$$C_{p\,min} = 1 + [(C_{pte} - 1)(Z + b)^{1/2}/a] = C_{p\,min}(Z,C_{pte},Re_{x0})$$

and therefore

$$C_{Lu} = -[C_{p\,min}(Z,C_{pte},Re_{x0})k_{lr} + I_s(Z,C_{pte},Re_{x0})]/(Z + k_{lr} - 1) \quad (33)$$

The conditions of Eqs. (28) and (31) become

$$\partial C_{Lu}/\partial Z = 0, \qquad \partial^2 C_{Lu}/\partial Z^2 < 0 \quad (34)$$

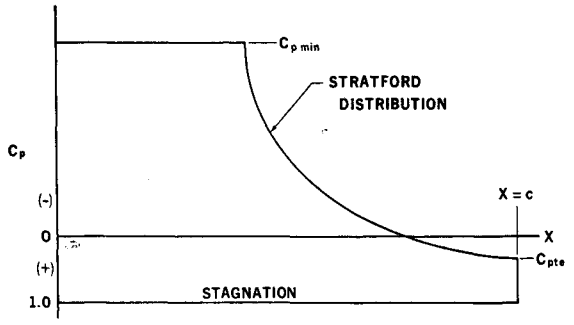

Fig. 6 Optimum airfoil pressure distribution according to variational analysis.

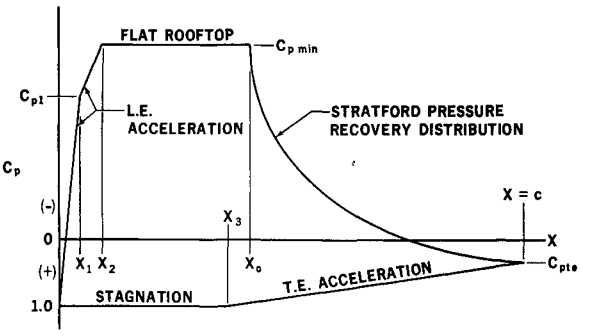

Fig. 7 Modified form of optimum pressure distribution for airfoil upper and lower surfaces, case a and case b (not to scale).

as conditions on Z for a maximum. Application of Eqs. (34) to Eq. (33) yields an analytic expression for Z as a function of C_{pte} and Re_{x0}. This completes the variational analysis of the upper-surface pressure distribution with the parameters C_{pte} and Re_{x0} left unspecified at this time.

Table 1 Coordinates for airfoil at design angle of attack (Laminar rooftop, $Re_\infty = 5 \times 10^6$)

Lower surface		Upper surface	
x/c	y/c	x/c	y/c
1.0	0.0	1.0	0.0
0.999	0.00035	0.999	0.000483
0.996	0.0014	0.996	0.001935
0.991	0.0032	0.991	0.00437
0.984	0.0057	0.984	0.0078
0.975	0.0090	0.975	0.00123
0.964	0.0131	0.964	0.0178
0.951	0.0180	0.951	0.0245
0.936	0.02375	0.936	0.0323
0.919	0.0304	0.919	0.0413
0.900	0.0381	0.900	0.0517
0.879	0.0468	0.879	0.0634
0.856	0.0566	0.856	0.0766
0.831	0.0676	0.831	0.0913
0.805	0.0793	0.805	0.1071
0.778	0.0919	0.778	0.1240
0.750	0.1053	0.750	0.1420
0.721	0.1197	0.721	0.1612
0.691	0.1349	0.691	0.1818
0.660	0.1511	0.660	0.2036
0.628	0.1682	0.628	0.2268
0.596	0.1857	0.596	0.2508
0.564	0.2036	0.564	0.2754
0.532	0.2217	0.532	0.3008
0.500	0.2399	0.500	0.3268
0.468	0.2580	0.468	0.3544
0.436	0.2756	0.436	0.3828
0.404	0.2916	0.404	0.4119
0.372	0.3047	0.372	0.4419
0.340	0.3144	0.340	0.4657
0.309	0.3201	0.309	0.4811
0.279	0.3231	0.279	0.4906
0.250	0.3243	0.250	0.4961
0.222	0.3241	0.222	0.4988
0.195	0.3228	0.195	0.4983
0.169	0.3202	0.169	0.4961
0.144	0.3163	0.144	0.4920
0.212	0.3109	0.121	0.4862
0.100	0.3041	0.100	0.4781
0.0810	0.2961	0.0810	0.4679
0.0640	0.2870	0.0640	0.4551
0.0490	0.2782	0.0490	0.4405
0.0360	0.2731	0.0360	0.4210
0.0265	0.2718	0.0250	0.3950
0.0195	0.2717	0.0160	0.3668
0.0130	0.2730	0.0090	0.3352
0.0095	0.2743	0.004	0.3075
0.0055	0.2775	0.001	0.2870
0.0025	0.2810		
0.001	0.2870		

2.6 Final Form of Airfoil Pressure Distribution

The variational analysis provides an idealized pressure distribution of the form shown in Fig. 6. Additional constraints, not employed in the optimization of the pressure distribution thus far, are necessary at this stage: 1) the airfoil must close at the trailing edge without having negative area, 2) the leading edge must be rounded to permit operation over an angle of attack range, and 3) the Kutta condition must be satisfied. These constraints are accommodated by providing a large finite acceleration on the upper surface near the leading edge, and a moderate acceleration on the lower surface near the trailing edge as shown in Fig. 7. For a given Re_{x0} (and hence Re_∞), the parameters X_1, X_2, X_3, C_{pl}, and C_{pte} will be adjusted to obtain an acceptable airfoil.

It is essential to note that the variational problem formulated in this study cannot lead to other than an infinite pressure gradient at the leading and trailing edtes as indicated in Fig. 6. The application of linear pressure variations near the leading and trailing edges was done arbitrarily, and is not part of the variational analysis. It is expected, however, that the inclusion of formal constraints that would limit the magnitude of the pressure gradient to some maximum value would lead to a linear pressure variation at that value of the gradient.

3. Results

Values of the upper-surface lift coefficient C_{Lu} calculated from Eq. (33) are shown in Fig. 8 for $10^6 \leq Re_\infty \leq 10^7$ and $0.1 \leq C_{pte} \leq 0.3$. The range of Re_∞ is obtained by varying Re_{x0} and using Eq. (8). C_{Lu} is seen to increase with Re_∞, and is significantly higher for case b than case a. The value of C_{pte} has a strong effect on C_{Lu}, and this influenced the procedure used in varying the parameters of the pressure distribution to obtain the airfoils. Actually, the selection of a value of C_{pte} involves a careful judgment of boundary-layer

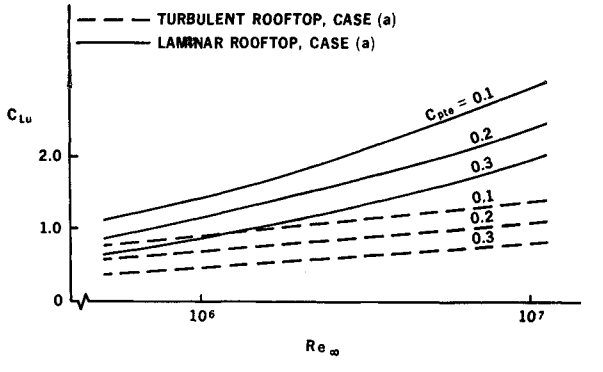

Fig. 8 Variation of C_{Lu} with Re_∞, case a and case b.

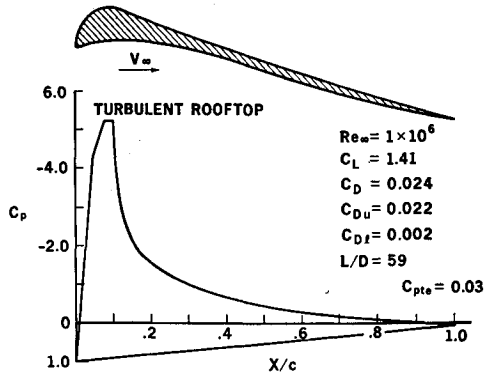

Fig. 9 Airfoil geometry and pressure distribution, turbulent rooftop, $Re_\infty = 10^6$.

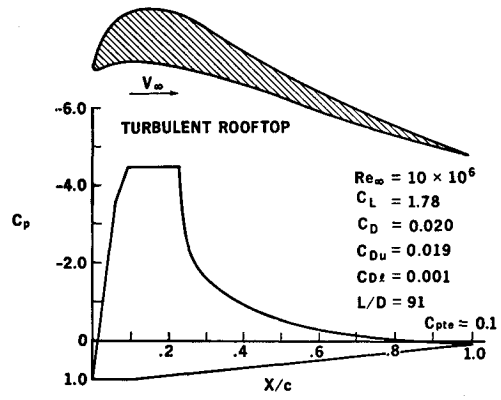

Fig. 11 Airfoil geometry and pressure distribution, turbulent rooftop, $Re_\infty = 10 \times 10^6$.

effects at the trailing edge, and much work remains to be done in this area.

Weber's inverse airfoil solution[4] was used to obtain the profiles. X_1, X_2, and C_{pl} were varied to obtain acceptable leading-edge geometry. C_{pte} and X_3 were used to control the aft portion of the airfoil geometry. For a particular value of C_{pte}, increasing X_3 caused the thickness near the trailing edge to decrease, and thus, the desired value of X_3 was that which just causes the airfoil to close. From Fig. 8, it is evident that the lowest value of C_{pte} is desired. It was found that if the value of C_{pte} was too low, the airfoil closed upstream of the trailing edge resulting in a reflexed profile. Therefore, the minimum allowable value of C_{pte} was considered to be that where the profile was not reflexed, and for practical purposes it was considered desirable to maintain a reasonable thickness distribution over the aft portion of the profile.

Figures 9–14 present the profile shapes obtained and their corresponding pressure distributions. Values of C_L, C_D, C_{Du}, and C_{Dl} are given for each. A list of coordinates for the airfoil of Fig. 13 is given in the Table 1. These were obtained by iterating from the profile predicted by the Weber theory using the Douglas Neumann potential-flow program[5] as a direct solution in order to obtain a more precise profile. The exact pressure distribution corresponding to this shape is also shown in Fig. 13.

The drag coefficients were calculated using the relation given by Thwaites in Ref. 3. The boundary layer was taken as laminar over the entire lower surface for the laminar rooftop airfoils, and turbulent for the turbulent rooftop airfoils. In addition, the drag for the airfoil of Fig. 13 has been calculated using the Douglas turbulent boundary-layer program.[6]

4. Conclusions

The family of optimum upper-surface pressure distributions effectively represent the maximum amount of lift which may be carried by the upper surface of a monoelement airfoil without separation. Since the Stratford theory on which they were developed has been verified experimentally in Ref. 2, such distributions and performance would appear to be attainable under actual flight conditions.

The airfoil profiles obtained using the Weber theory are, of course, only approximate. They do, however, indicate that the proposed optimum pressure distributions provide realistic airfoil sections. The leading-edge acceleration regions required for the airfoils of Figs. 9–14 caused more of a reduction in the lift coefficient than was expected, particularly for the airfoils of case a. This is probably a result of using the Weber method for computing the airfoil profiles, and therefore steeper leading-edge accelerations should be acceptable when a more accurate inverse technique is employed. On the other hand, the lower-surface acceleration region proved to be quite reasonable in its linear form. Attempts to increase the lift coefficient by assuming more arbitrary forms failed to provide any significant improvement.

The trend of increasing lift coefficient with Reynolds number is as expected. Compressibility induced separation effects have not been directly considered. However, since the load has been spread over the maximum chordwise distance possible, the airfoils should have relatively high critical Mach numbers at the design condition. Theoretical predication of the drag coefficients is somewhat speculative because of the special form of the pressure distributions. Nevertheless, the agreement between the results obtained using Thwaites' method and the Douglas turbulent boundary-layer program for the airfoil of Fig. 13 suggests that these results may be realistic.

In this analysis, separation has not been permitted anywhere on the airfoil. As a result, the drag coefficients predicted theoretically by Thwaites' formula are quite low, and

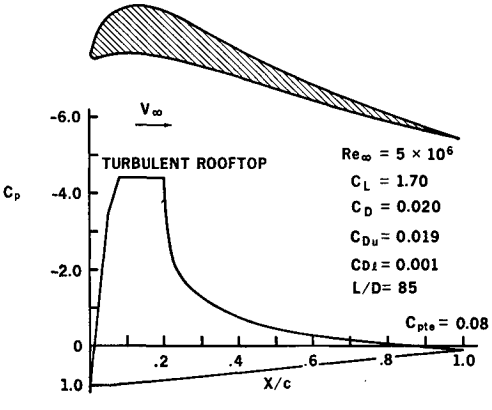

Fig. 10 Airfoil geometry and pressure distribution, turbulent rooftop, $Re_\infty = 5 \times 10^6$.

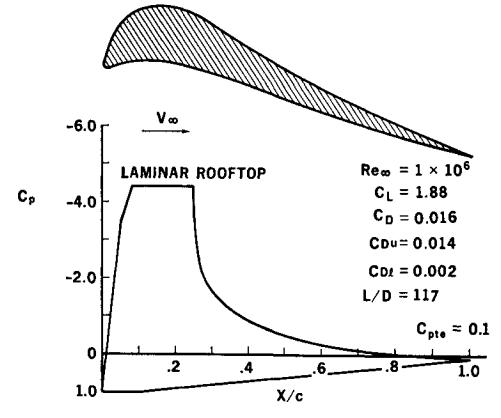

Fig. 12 Airfoil geometry and pressure distribution, laminar rooftop, $Re_\infty = 10^6$.

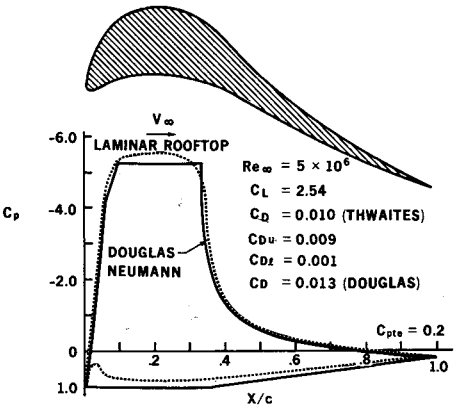

Fig. 13 Airfoil geometry and pressure distribution, laminar rooftop, $Re_\infty = 5 \times 10^6$.

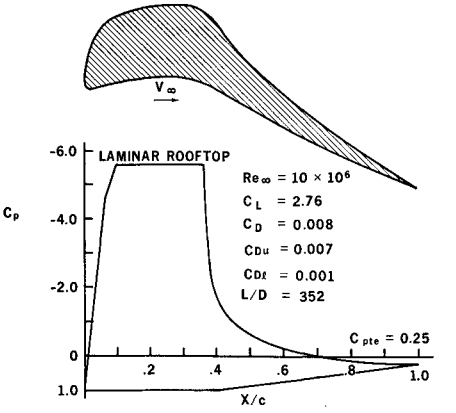

Fig. 14 Airfoil geometry and pressure distribution, laminar rooftop, $Re_\infty = 10 \times 10^6$.

thus, the airfoils provide a high L/D at high C_L. Such performance may be particularly useful in, for instance, V/STOL, long endurance, and man-powered flight applications. On the other hand, $C_{L\,\max}$ is classically defined as that value of the lift coefficient when the slope of the lift curve equals zero, and almost all airfoils are partially separated at this point. Therefore, since it has been shown that C_{pte} has a strong effect on C_{Lu}, it is possible that by designing an airfoil with limited separation at the trailing edge, significantly higher-lift coefficients could be obtained. Naturally, these more sophisticated applications will require the inclusion of boundary-layer thickness effects, particularly near the trailing edge.

A planned extension of this work will be to apply an exact inverse solution to obtain the profiles. This will allow a more precise definition of leading and trailing-edge conditions and should, if anything, improve the performance. The resulting airfoils will then be evaluated in an experimental program.

References

[1] Stratford, B. S., "The Prediction of Separation of the Turbulent Boundary Layer," *Journal of Fluid Mechanics*, Vol. 5, 1959.

[2] Stratford, B. S., "An Experimental Flow with Zero Skin Friction Throughout its Region of Pressure Rise," *Journal of Fluid Mechanics*, Vol. 5, 1959.

[3] Thwaites, B., ed., *Incompressible Aerodynamics*, Oxford, 1960.

[4] Weber, J., "The Calculation of the Pressure Distribution on the Surface of Thick Cambered Wings and the Design of Wings with Given Pressure Distribution," RM No. 3026, June 1955, Aeronautical Research Council, London, England.

[5] Hess, J. L. and Smith, A. M. O., "Calculation of Potential Flow About Arbitrary Bodies," *Progress in the Aeronautical Sciences*, edited by D. Kuchemann, Vol. 8, Pergamon Press, New York, 1966.

[6] Cebeci, T. and Smith, A. M. O., "A Finite-Difference Solution of the Incompressible Turbulent Boundary-Layer Equations by an Eddy-Viscosity Concept," *1968 Symposium on Turbulent Boundary Layers*, Stanford, Calif., Aug. 1968.

SYNOPTIC: Jet Circulation Control Airfoil for VTOL Rotors, S. W. Yuan, George Washington University, Washington, D.C.; *Journal of Aircraft,* Vol. 7, No. 5, pp. 417–423.

Experimental Investigation of Circulation Control Airfoils by Means of Jets

Theme

This paper presents experimental investigations of the basic aerodynamic characteristics of elliptical airfoils with jet circulation control for VTOL rotors. The flow past an airfoil with an oscillating blowing jet was also investigated. These results were used to compare with available theories as well as other experimental data.

Content

The purpose of this investigation is to study the basic aerodynamic characteristics of elliptical airfoils with jet circulation control for VTOL rotors. Based on the potential flow theory calculation, the capacity of the air supply, the limitation of the compressibility effect of the jet stream at high velocities, the elliptical airfoils of 18 and 12% thickness ratios were designed and constructed. Experimental investigations for both models with trailing-edge jets include force and pitching moment measurements. In addition, static pressure measurements were made in both spanwise and chordwise directions.

Circulation control with dual jets for the elliptical airfoil of 18% thickness ratio was tested with very satisfactory results. The determination of the aerodynamic response of the airfoil model to cyclic changes in jet mass flow was also made. The cyclic results were very satisfactory and are presented in the form of pulsating lift coefficient, drag coefficient, and pressure coefficient as a function of pulsating jet coefficient.

The results of this investigation, performed in a 22 × 36 in. wind tunnel at Reynolds number up to 10^6, can be summarized as follows:

1) The maximum lift coefficient $C_L = 3.45$ ($C_J = 1.32$), at zero angle of attack was obtained for the elliptical airfoil of 18% thickness ratio. However, at 4° angle of attack the maximum lift coefficient increased to 4.2 at the same C_J.

2) Static pressure distributions in the chordwise direction for elliptical airfoils of both 18% and 12% thickness ratios were measured at various values of C_J. Several measured pressure distributions were compared with the corresponding theoretical values. These two sets of values for pressure distributions were considered to be in reasonably good agreement.

3) The section drag coefficient of the elliptical airfoil with trailing-edge jet is obtained by taking the difference of the measured values of the jet thrust coefficient and the corresponding calculated values. It appears that the section drag coefficient of the elliptical airfoil is comparable with that of NACA 0012 airfoil for the range of lift coefficients less than 1.4. Beyond this value of lift coefficient, the section drag of the elliptical airfoil is much smaller than that of NACA 0012 section (Fig. 1).

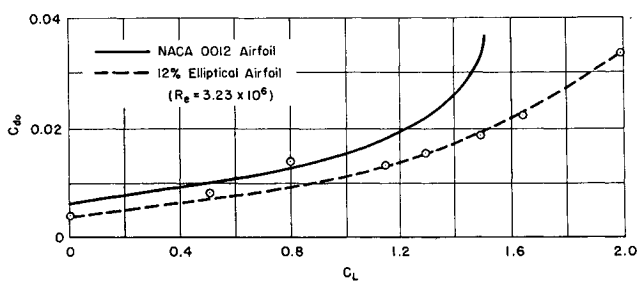

Fig. 1 Comparison of section drag coefficient.

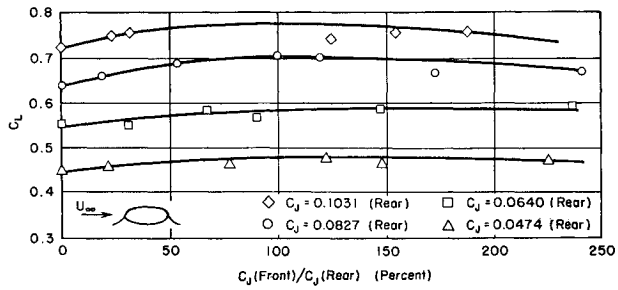

Fig. 2 Total lift coefficient vs ratio of leading-edge jet coefficient to trailing-edge jet coefficient (18% thickness ratio).

4) One of the most encouraging results was obtained from an experiment performed on the elliptical airfoil of 18% thickness ratio with dual jets (both leading-and trailing-edge jets are used). The results indicated that the leading-edge jet did not disturb the incoming flow and actually furnished some additional reaction force to the lift (Fig. 2). As a consequence, if the elliptical airfoil with dual jets is used for the rotor blades, the loss of lift in the reverse flow region can be completely eliminated.

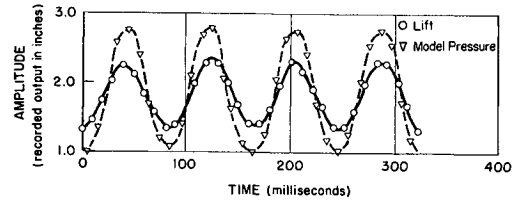

Fig. 3 Pulsating lift and model pressure for elliptical airfoil of 18% thickness ratio (valve speed = 360 rpm).

5) The results of aerodynamic response measurements of the elliptical airfoil to cyclic changes in the blowing jet were surprisingly encouraging. The cyclic valve was tested at frequencies up to 12/cps and the response of the lift was found to be excellent, with very little delay (Fig. 3). The response of the drag as well as the chordwise pressure distribution to the cyclic changes in the blowing jet were also found to be good. These results clearly indicate that the periodic variation of lift on the blade of a VTOL rotor can be obtained by a cyclic variation of the jet momentum; hence, the circulation control problem is reduced to simply the problem of regulating the mass flow (both cyclically and collectively) from the power source.